# Adaptive Cold-Load Pickup Considerations in 2-Stage Microgrid Unit Commitment for Enhancing Microgrid Resilience

Rongxing Hu, Ashwin Shirsat, Valliappan Muthukaruppan, Yiyan Li, Si Zhang, Wenyuan Tang, Mesut Baran, Ning Lu*

*Electrical & Computer Engineering Department, Future Renewable Electric Energy Delivery and Management (FREEDM) Systems Center, North Carolina State University, Raleigh, NC 27606 USA*

**Abstract:** In an extended main grid outage spanning multiple days, load shedding serves as a critical mechanism for islanded microgrids to maintain essential power and energy reserves that are indispensable for fulfilling reliability and resiliency mandates. However, using load shedding for such purposes leads to increasing occurrence of cold load pickup (CLPU) events. This study presents an innovative adaptive CLPU model that introduces a method for determining and incorporating parameters related to CLPU power and energy requirements into a two-stage microgrid unit commitment (MGUC) algorithm. In contrast to the traditional fixed-CLPU-curve approach, this model calculates CLPU duration, power, and energy demands by considering outage durations and ambient temperature variations within the MGUC process. By integrating the adaptive CLPU model into the MGUC problem formulation, it allows for the optimal allocation of energy resources throughout the entire scheduling horizon to fulfill the CLPU requirements when scheduling multiple CLPU events. The performance of the enhanced MGUC algorithm considering CLPU needs is assessed using actual load and photovoltaic (PV) data. Simulation results demonstrate significant improvements in dispatch optimality evaluated by the amount of load served, customer comfort, energy storage operation, and adherence to energy schedules. These enhancements collectively contribute to reliable and resilient microgrid operation.

***Keywords*:** cold load pickup, load shedding, microgrid, reconfiguration, resilience service, unit commitment.

**Nomenclature**

***Notations for the 1st stage MGUC***

| | |
|---|---|
| $l, m, n$ | Load group (LG) index |
| $N^{\mathrm{G}}$ | Number of LGs |
| $lm, mn$ | Index of the switch connecting LG $m$ and $n$ |
| $p$ | Phase index |
| $\Delta t, t, N_t$ | Time interval (30min), interval index, and the number of intervals |
| $f_1^{\mathrm{load}}$ | Total weighted load served |
| $f_1^{\mathrm{PV}}, c^{\mathrm{PV}}$ | PV curtailment and its penalty factor |
| $f_1^{\mathrm{CLPU}}$ | Total CLPU penalty |
| $w_{m,p}^{\mathrm{crit}}, w_t^{\mathrm{pref}}$ | Weightings of critical loads and loads during customer preferred supply periods |
| $U_{m,t}^{\mathrm{G}}, U_{m,t}^{\mathrm{Goff}}$ | Supply status and interruption status of the LG $m$, binary |
| $P_{m,p,t}^{\mathrm{Ncrit}}, P_{m,p,t}^{\mathrm{crit}}$ | Non-critical load and critical load forecasts without CLPU effect, i.e., the corresponding steady-state or normal loads |
| $P_{\mathrm{PV},t}^{\mathrm{pred}}$ | PV prediction |
| $P_{\mathrm{PV},t}, P_{\mathrm{PV},t}^{\mathrm{curt}}$ | Scheduled PV utilization and curtailment |
| $T_t^{\mathrm{out}}$ | Outdoor temperature |

* Corresponding author. *E-mail address:* nlu2@ncsu.edu.

| | |
|---|---|
| $P_{m,t}^{\text{Steady}}$ | Normal TCL load when no outages |
| $P_{m,p}^{\text{MaxCLPU}}$ | Synchronized peak of TCLs |
| $D_{m,t}^{\text{peaksatu}}$ | Saturated peak duration under the temperature of interval *t* |
| $\tau_{m,t}^{\text{Tout}}$ | CLPU peak duration increment under the temperature of interval *t* |
| $U_{m,t}^{\text{satu}}$ | Saturation status of the estimated CLPU peak duration, binary |
| $d_{m,t}$ | Accumulated CLPU peak duration during outages without considering saturation |
| $d_{m,t}^{\text{peak}}$ | Accumulated CLPU peak duration during outages considering saturation |
| $d_{m,t}^{\text{re}}$ | Remaining peak duration at the beginning of interval *t* |
| $\gamma_{m,t}^{\text{Tout}}$ | CLPU power decay rate |
| $U_{m,t}^{\text{decay}}$ | CLPU decay status |
| $k_{m,t}, k_{m,t}^{\text{Steady}}$ | Factors of TCL load and normal TCL load, in per unit value |
| $k_{m,t}^{\text{CLPU}}, P_{m,p,t}^{\text{CLPU}}$ | CLPU consumption in per unit value (factor) and in kW |
| $P_{m,p,t}^{\text{norm}}$ | Normal load in LG *m* on phase *p* when no outages |
| $\Omega_m^{\text{from}}, \Omega_m^{\text{to}}$ | The "from" LG set and "to" LG set of the LG *m* |
| $P_{mn,p,t}$ | Active power at switch *mn* flowing from LG *m* to LG *n* |
| $c_{\text{e}}^{\text{CLPU}}, c_{\text{dp}}^{\text{CLPU}}, c_{\text{re}}^{\text{CLPU}}$ | Penalty factors of CLPU increment, CLPU peak duration and remaining peak duration |
| $D_{m,\text{ini}}^{\text{MSD}_{\text{served}}}$ | The initial service duration of the current scheduling horizon |
| $D_m^{\text{MSD}}, \widehat{D}_{m,t}$ | Consecutive scheduling intervals corresponding to the MSD and the required service duration |
| $x, N^{\text{topol}}$ | Topology index and the number of topology candidates |
| $U_{x,t}^{\text{topol}}$ | Selection status of the $x^{\text{th}}$ topology candidate, binary |
| $\mathcal{M}_t^{\text{G}}$ | Mapping matrix of distribution network topology candidates and LG status, $N^{\text{G}} \times N^{\text{topol}}$ |
| ***Notations for the 2nd stage MGUC*** | |
| $i, N_m^{\text{node}}$ | Node index and the number of nodes in LG *m* |
| $\Delta t', T_2$ | Interval and horizon of the 2nd stage |
| $f_2^{\text{DR}}$ | DR usage |
| $f_2^{\text{PV}}, c_2^{\text{PV}}$ | PV curtailment and its penalty factor |
| $f_2^{\text{BESS}}, c_2^{\text{low}}$ | BESS negative energy deviation penalty and its penalty factor |
| $U_{m,i,p,t'}^{\text{DR}}$ | Load shedding status of node *i*, binary |
| $P_{m,i,p,t'}^{\text{node}}, P_{m,i,p,t'}^{\text{norm}}$ | Total load and the normal load of node *i* |
| $k_{m,t'}^{\text{CLPU}}$ | CLPU factor for the 2nd stage |
| $E_1$ | BESS energy setpoint, i.e., the BESS energy by the end of the first step from the 1st stage MGUC |
| $E_{2,T_2}$ | BESS energy by the end of the last step at the 2nd stage |
| $\Delta E_2^{\text{low}}$ | BESS negative energy deviation |

## 1. Introduction

The increase in severe weather events across the United States has resulted in a higher frequency of extended power outages spanning multiple days [1]. This trend has sparked increased attention toward advancing microgrid technology as a means to bolster the robustness of electricity services [2]. To ensure power supply during extended outages that last for multiple days, the creation of temporary microgrids presents more economically viable options compared to the implementation of self-contained permanent microgrids, primarily because multi-day outages occur with low probabilities.

However, within temporary microgrids reliant on highly intermittent generation resources and battery energy storage systems (BESS), which are likely to constitute the majority of DERs in distribution systems [3], the installed capacity of intermittent DERs often proves inadequate for sustaining all loads during prolonged outages spanning multiple days. As a result, microgrid unit commitment (MGUC) frequently requires multiple load shedding actions through demand response or feeder reconfiguration. These measures are crucial for upholding

the availability of essential power and energy reserves to meet reliability and resilience requirements.

Nevertheless, in scenarios where the shed loads include a significant proportion of thermostatically controlled loads (TCLs), such as Heating, Ventilation, and Air Conditioning (HVAC) units, the TCLs' temperature can gradually shift away from the desired range. As a result, when the interrupted loads are reconnected, all TCLs might activate simultaneously. Furthermore, restoring the TCLs' temperature will require the devices to operate for periods ranging from tens of minutes to hours beyond their usual cycling durations. This situation leads to a notable surge in peak power demand and additional energy requirements, which is known as the cold load pickup (CLPU) phenomenon.

Given that TCLs usually account for around 50% of energy usage in distribution systems [4] in cold winter or hot summer days, the impact of CLPU becomes particularly significant when scheduled interruptions extend for hours or overnight. Consequently, MGUC algorithms must factor in CLPU requirements while planning load shedding by reconfiguration to fulfill power and energy demands. We will now examine the current state-of-the-art concerning the existing CLPU model and its application within MGUC for the purpose of optimizing the scheduling of service restoration and load shedding events.

**Existing CLPU Models:** Two approaches have been proposed in the literature for modeling CLPU: data-driven and model-based. The data-driven methodology calculates the CLPU curve through historical outage data. For instance, curve-fitting methods can compute the CLPU peak for various outage durations [5]. Another approach involves predicting the CLPU peak from a statistical CLPU model [6]. The limitation of these approaches is the insufficient outage data available for model derivation.

The *model-based* approach uses physics TCL models to estimate CLPU effects. A CLPU delayed exponential model is proposed in [7] based on heating load simulation under a specified outside ambient temperature. In [8], a 3-piecewise linear function that depicts the CLPU power consumption of the CLPU peak period and the decay period is presented, the exponential decay is simplified to a linear decay. Many widely used delayed exponential models or their linearized versions yield **a fixed CLPU profile** computed from fixed ambient temperature and outage duration. However, in practice, ambient temperature is time-varying and load shedding duration is unknown before the MGUC has been solved. Thus, a fixed CLPU model only yields the rough estimation of CLPU power and energy needs in MGUC. In [9], the authors present a multi-state load model that estimates the CLPU peak and the CLPU duration using TCL status and settings as inputs. However, if detailed TCL-level information is not available to the microgrid controller, the methods cannot be applied.

In summary, when estimating CLPU power (e.g., peak power, duration, decay rate, and steady-state power) and energy needs, the existing CLPU models cannot account for variable interruption duration and time-varying ambient temperature changes [10].

**MGUC enhanced by CLPU Constraints:** As shown in Table I, various methods have been proposed to incorporate the CLPU considerations into MGUC. For example, in [11], the authors propose to use a linearized, delayed exponential CLPU curve to formulate a Mixed-Integer Linear Programming (MILP) algorithm for service restoration by microgrids. An alternative approach proposed by authors in [12-13] represents CLPU as a separate demand block for coordinative scheduling of service restoration and repair crew routing. In [14-15], the authors use interruption duration as an input for selecting a CLPU profile from a set of predefined candidate profiles. These profiles are generated by simulating CLPU effects under different interruption durations while maintaining a consistent outdoor temperature. Also, the CLPU power fluctuation when outages are short and some houses' temperatures are still within comfort bands is considered [14], and uncertainties of CLPU curves are modeled by adding Gaussian noise to the selected CLPU profile [15]. The main disadvantage of methodologies outlined in [11-15] is their underlying assumption of *a constant ambient temperature throughout the duration of the CLPU period*. Additionally, the authors use MGUC for microgrid load restoration, they assume once a cold load is picked up, it cannot be re-interrupted. Thus, in the problem formulation *the MGUC only needs to accommodate one complete CLPU event for a scheduling horizon*.

However, when dealing with the scheduling of multiple service interruptions to fulfill power and energy reserve needs during prolonged outages, the timing and duration of the load shedding events are decision variables. Moreover, if the load shedding event lasts for hours or overnight, using a fixed ambient temperature throughout

the entire period will result in large errors in CLPU estimation. Thus, if the MGUC is required to optimize when, how many, and how long the load shedding events are, relying solely on a limited set of fixed CLPU profiles proves inadequate. This is because the variability in ambient temperature and outage durations can span a wide range in a prolonged scheduling period (e.g., 24 or 48 hours). For instance, the temperature can fluctuate by more than 10°C, and outages may vary between 2 and 14 hours. Likewise, creating a set of predefined candidate CLPU profiles becomes impractical due to the necessity for a significantly large number of candidates to adequately address the scheduling requirements. Thus, in this paper, we present an adaptive CLPU model, which can be directly integrated into the MGUC, for estimating the power and energy requirements of multiple CLPU events. In Table I, we highlight the unique considerations of the proposed CLPU enhanced MGUC algorithm and provide a comprehensive comparison with the existing methods.

The main contributions of the paper are two-fold. First, we introduce an adaptive CLPU model that can accurately estimate CLPU using interruption duration and ambient temperature as inputs. The CLPU model parameters can be estimated offline using TCL parameters derived from the smart meter data for a wide range of operation conditions. Second, we present the formulation of the adaptive CLPU based operational constraints, which can be integrated into a 2-stage MGUC formulation for optimal scheduling of multiple load shedding events. This enables the microgrid to optimize the number, timing and duration of the load shedding events, consequently leading to more optimal power and energy dispatch outcomes during extended outages in multi-day microgrid operation. The adaptive CLPU enhanced MGUC is formulated as a MILP problem, making it tractable, and its performance is verified by real-time device level CLPU simulation.

The rest of this paper is organized as follows. Section 2 presents the proposed adaptive CLPU model and the proposed MGUC algorithm considering adaptive CLPU estimation. Results are presented in Section 3 and Section 4 concludes the paper.

Table I. Summary of literature review

| Ref. | Microgrid Operation Setup | | | Microgrid Unit Commitment Algorithm Setup | | | | | | Verified dynamic responses § |
|---|---|---|---|---|---|---|---|---|---|---|
| | 3-phase unbalanced system | Outage duration | Main energy source* | Optimization stages | Rolling horizon | Forecast error | **CLPU** Y/N | CLPU events | CLPU model | |
| [11] | | < 1 hour | DG | RT | ✓ | | ✓ | one | fixed | no real-time CLPU simulation |
| [12] | | up to days | DG | DA | | ✓ | ✓ | one | fixed | |
| [13] | ✓ | up to days | DG + BESS | DA | | ✓ | ✓ | one | fixed | |
| [14] | ✓ | several hours | DG | RT | | ✓ | ✓ | one | candidate | |
| [15] | | several hours | DG | RT | | ✓ | ✓ | one | candidate | |
| [16] | | several hours | DG | DA | | ✓ | | multiple | | |
| [17] | | < 1 day | DG | DA+RT | | ✓ | | multiple | | |
| [18] | ✓ | < 1 hour | DG | RT | | | | one | | |
| [19] | ✓ | up to days | DG | DA | | | | multiple | | no CLPU |
| [20] | ✓ | < 1 day | DG + BESS | DA | ✓ | | | multiple | | |
| [21] | ✓ | several hours | DG + BESS | RT | | | | multiple | | |
| [22] | | multi-days | BESS + PV | DA | | | | multiple | | |
| **Proposed** | ✓ | **multi-days** | **BESS + PV** | **DA+RT** | ✓ | ✓ | ✓ | **multiple** | **adaptive** | **verified by real-time CLPU simulation** |

*DG denotes dispatchable distributed generations; § Using openDSS, gridLAB or HIL simulation

## 2. Methodology

In this section, we present the CLPU model and the integration of the CLPU constraints into the MGUC algorithm for multi-day, off-grid operation.

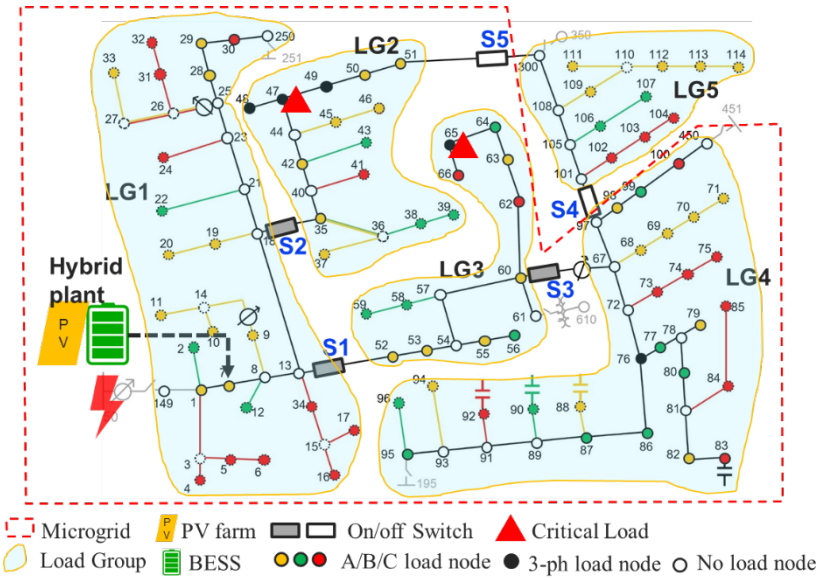


Fig. 1. Configuration of the microgrid test system (when serving LGs 1-4).

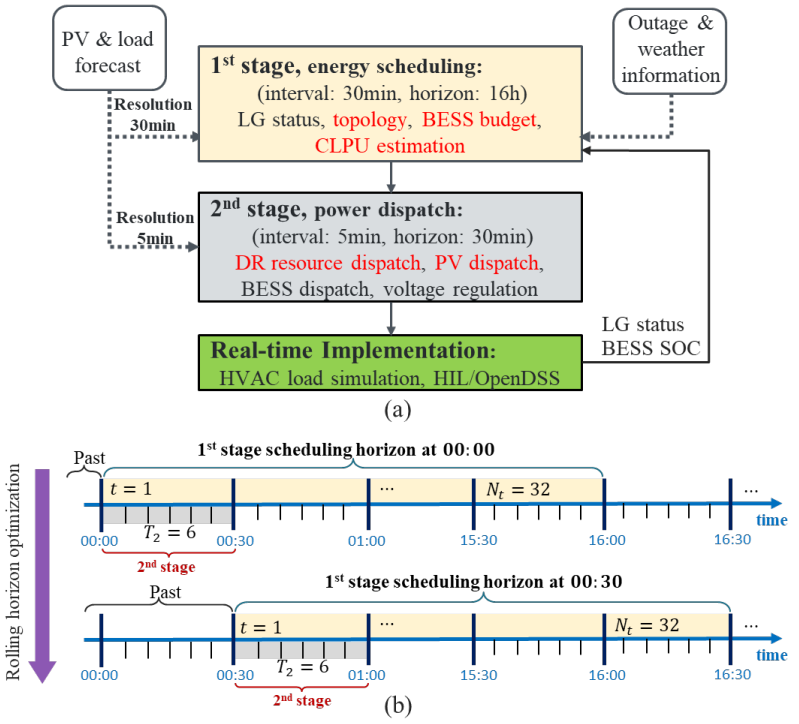


Fig. 2. The Two-Stage MGUC Process: (a) Flowchart of the 2-Stage MGUC, with commands sent to the next stage marked in red, and (b) Scheduling Horizons and Intervals for the 1st and 2nd Stages.

## 2.1 Overview of the Feeder-level Microgrid Operation

In this paper, a modified IEEE 123-bus test system [23] is used to illustrate the feeder-level temporary microgrid operation. As shown in Fig. 1, a hybrid energy system consisting of a MW-level photovoltaic (PV) plant and a grid-forming BESS is connected to bus 7. Five 3-phase switches (S1-S5) can be used to remotely switch on/off the five load groups (LG1-LG5). LG2 and LG3 are critical LGs as they serve critical loads. Please note that critical loads are assumed to have dedicated backup generators, but they still have high supply priority for preserving their fuel.

A 2-stage MGUC is used to schedule the microgrid operation, as shown in Fig. 2(a). A *16-hour ahead*

*rolling forecaster* and a *30-minute ahead forecaster* provide the PV, load, and weather forecasts to the 1st and 2nd stage MGUC, respectively. In the 1st stage, a *rolling 16-hour ahead MGUC* is conducted every 30 minutes to schedule BESS, PV, and the on/off status of LGs and switches. The solution for the first 30-minute interval will be executed and used as the inputs for the 2nd stage MGUC.

As shown in Fig. 2(b), each scheduling interval is 30-minute ($\Delta t = 30$) so there are 32 scheduling intervals ($N_t$ =32) in the 1st stage MGUC. As the BESS is the only grid-forming device in the microgrid, we assume that load shedding, achieved by switching LGs off, is the main approach for meeting power reserve requirements and energy needs. In the 2nd stage, all weather variables are treated as static. The circuit topology, BESS budget, and CLPU estimations derived from the 1st stage MGUC for the forthcoming 30-minute interval are transmitted to the 2nd stage MGUC, where intra-30-minute, 5-minute-interval power dispatch decisions are made for BESS and DR to ensure load balance and voltage regulation. This two-stage process, using a rolling horizon optimization strategy, is performed every 30 minutes, as illustrated in the timeline diagram in Fig. 2 (b).

### 2.2 Problem Formulation for the 1st Stage

The objective function of the 1st stage is formulated as

$$\max \ f_1^{\text{load}} - c^{\text{PV}} f_1^{\text{PV}} - \boldsymbol{f_1^{\text{CLPU}}} \tag{1}$$

$$f_1^{\text{load}} = \sum_{t=1}^{N_t} \sum_{m=1}^{N^{\text{G}}} \sum_{p\in\{a,b,c\}} U_{m,t}^{\text{G}} w_t^{\text{pref}} \left(P_{m,p,t}^{\text{Ncrit}} + w_{m,p}^{\text{crit}} P_{m,p,t}^{\text{crit}}\right) \Delta t \tag{2}$$

$$f_1^{\text{PV}} = 3 \sum_{t=1}^{N_t} P_{\text{PV},t}^{\text{curt}} \Delta t \tag{3}$$

$$P_{\text{PV},t}^{\text{curt}} = P_{\text{PV},t}^{\text{pred}} - P_{\text{PV},t} \tag{4}$$

$$\sum_{x=1}^{N^{\text{topol}}} U_{x,t}^{\text{topol}} = 1 \tag{5}$$

$$\left[U_{1,t,}^{\text{G}} U_{2,t,}^{\text{G}} \dots U_{N^{\text{G}},t}^{\text{G}}\right]^{\top} = \mathcal{M}_t^{\text{G}} \left[U_{1,t,}^{\text{topol}} U_{2,t,}^{\text{topol}} \dots U_{N^{\text{topol}},t}^{\text{topol}}\right]^{\top} \tag{6}$$

$$\widehat{D}_{m,t} = \begin{cases} \min\left\{D_m^{\text{MSD}} - D_{m,\text{ini}}^{\text{MSD}_{\text{served}}}, N_t\right\}, t = 1 \\ \min\left\{D_m^{\text{MSD}}, N_t - t + 1\right\}, t > 1 \end{cases} \tag{7}$$

$$\sum_{z=0}^{\widehat{D}_{m,t}-1} U_{m,t+z}^{\text{G}} \geq \widehat{D}_{m,t} \left(U_{m,t}^{\text{G}} - U_{m,t-1}^{\text{G}}\right) \tag{8}$$

Equations (5) and (6) are reconfiguration constraints. We use a topology look-up table for selecting feasible and radial circuit topologies. We put all 13 feasible circuit topology candidates of the test system into a look-up table ($\left[U_{1,t,}^{\text{topol}} U_{2,t,}^{\text{topol}} \dots U_{N^{\text{topol}},t,}^{\text{topol}}\right]^{\top}$) so that a matching matrix ($\mathcal{M}_t^{\text{G}}$) can be used for determining the on/off of load groups ($U_{i,t,}^{\text{G}}$), the switch status can be determined using the similar methods. Equations (7) and (8) consider the minimum service duration (MSD) [22] to avoid frequent switching on/off LGs.

Note that the main objective of a conventional 1st stage MGUC is to maximize the total served load ($f_1^{\text{load}}$), minimize the PV curtailment ($P_{\text{PV},t}^{\text{curt}}$), and meet user comfort requirements (e.g., supply priority to critical loads and user-preferred hours, minimum service duration [22]). Our contribution to the MGUC problem formulation is the integration of CLPU energy constraints ($\boldsymbol{f_1^{\text{CLPU}}}$) into the existing MGUC objective function in (1). Then,

when scheduling the on/off status of an LG through feeder reconfiguration (i.e., determine $U^{G}_{m,t}$ in (2) considering constraints (5)-(8)), we can factor in the CLPU energy needs associated with re-energizing loads that were previously shed during subsequent intervals.

We will show in the simulation results that such considerations are crucial for multi-day microgrid operations, especially when the LGs need to be turned off multiple times. This is because, within a 30-minute interval, if the unaccounted CLPU energy requirement surpasses the allocated amount scheduled by the first-stage MGUC, the microgrid will exceed the "optimal" energy quota for that interval. Consequently, because of the overuse, the microgrid will fail to supply the scheduled loads in the subsequent 30-minute intervals.

Moreover, if the CLPU power demand exceeds the capacity of the available power supply, the microgrid would either need to unexpectedly shed load or be forced to shut down. We will introduce the CLPU power constraints in Section 2.4.

Please refer to [22] for the rest of the MGUC constraints, including PV and BESS operational constraints, microgrid reserve constraints, and polygon-based linearization of active power and reactive power constraints of the inverters and switches.

### 2.3 Adaptive CLPU Model

To illustrate the derivation of the adaptive CLPU model, we consider a scenario of 1100 heterogeneous HVAC units in the 123-bus test system. These HVAC units are modeled using the RCQ model introduced in [24]. To model realistic HVAC operation, we derive the RCQ parameters from 145 sets of sub-metered HVAC profiles (Pecan Street dataset [25]) using the method described in [26]. Note that in cases where sub-metered HVAC profiles are not available, the load disaggregation algorithms introduced in [27-28] can be used to extract the HVAC profiles from smart meter data.

Using those typical HVAC model parameters, we conduct offline simulations by using weather forecast and LG on/off status as inputs to model the HVAC load curve under different outdoor temperatures and scheduled interruption durations. As shown in Figs. 3 and 4, compared to the normal HVAC electricity consumption ($P^{\text{Steady}}_{m,t}$) when there are no service interruptions, a significant amount of extra energy will be needed for picking up the HVAC units that have been in the "off" state for an extended period. This additional energy corresponds to the CLPU energy requirements.

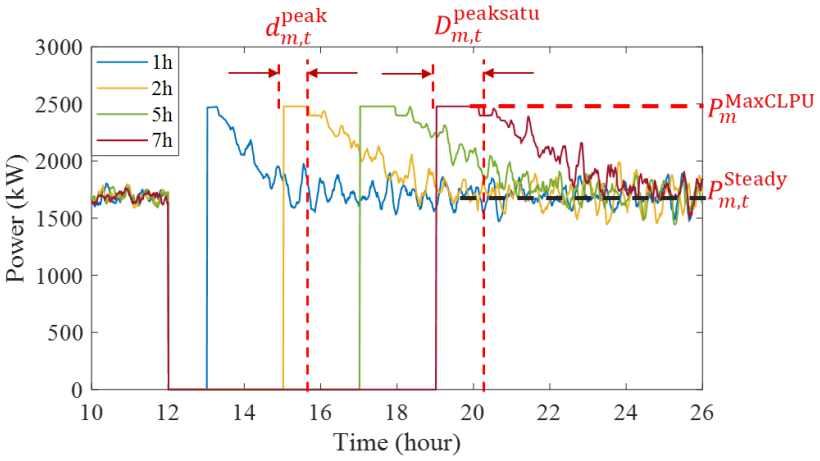


Fig. 3. CLPU curves for different outage lengths ($T^{\text{out}}$ =36 °C).

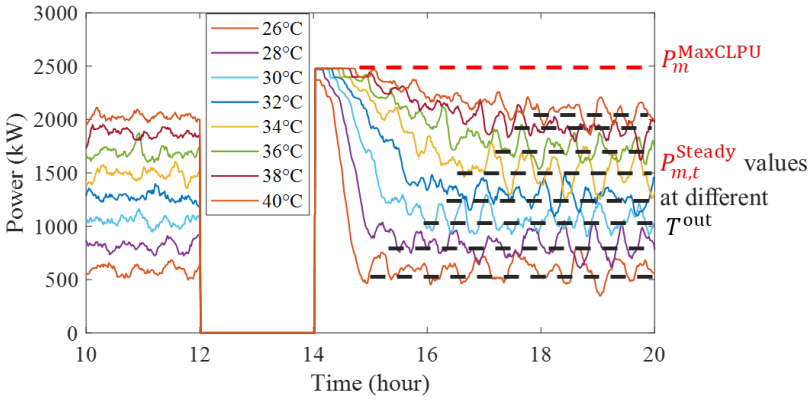


Fig. 4. CLPU curves for different outdoor temperatures (2-hour outage).

*Step 1: Compute the HVAC steady state power consumption at time interval t.* The TCL normal/steady-state load ($P_{m,t}^{\text{Steady}}$) can be readily estimated based on the outdoor temperature, as shown in Fig. 4.

*Step 2: Compute the CLPU peak power*. From the simulation results shown in Figs. 3 and 4, the peak CLPU power usually equals the synchronized peak of all HVAC loads, $P_m^{\text{MaxCLPU}}$. Although in mild days, a few HVACs don't need to work after resupply since their room temperatures could be still within the comfort bands, the CLPU peak can be slightly lower than $P_m^{\text{MaxCLPU}}$ (e.g., the 26 ºC case in Fig. 4), such cases can be ignored for hot summer or cold winter days. Thus, to simplify the CLPU model, in this paper, we assume that the CLPU peak will be equal to $P_m^{\text{MaxCLPU}}$. By doing so, our underlying assumption is that when a group of HVACs is off for more than 30 minutes, they will all turn on simultaneously when the power supply is restored. This assumption can lead to a slight overestimation of the power needs in mild days.

*Step 3: Compute the CLPU peak duration*. As shown in Figs. 3 and 4, the peak duration is dependent on the interruption duration and ambient temperature. As summarized in Fig. 5, at a given outdoor temperature, $T_t^{\text{out}}$, the CLPU peak duration, $d_{m,t}^{\text{peak}}$, is a function of outage/interruption duration, $d_{m,t}^{\text{off}}$. The longer the outage lasts, the longer the CLPU peak duration will be. To simplify the calculation, we linearize the $d_{m,t}^{\text{peak}}$ versus $d_{m,t}^{\text{off}}$ curve so that for a given temperature at interval $t$, an incremental peak duration can be calculated from the slope of the curve, $\tau_{m,t}^{\text{Tout}}$. Note that if the outage duration reaches a certain value, $d_{m,t}^{\text{offsatu}}$, $d_{m,t}^{\text{peak}}$ is capped at $D_{m,t}^{\text{peaksatu}}$. We opt for a 2-piece linearization to make a compromise between accuracy and problem complexity. Note that the 2-piece linearized curve can effectively capture the two primary characteristics of the CLPU curve: 1) the CLPU peak duration increases as the outage duration increases, 2) the CLPU peak has a saturation point.

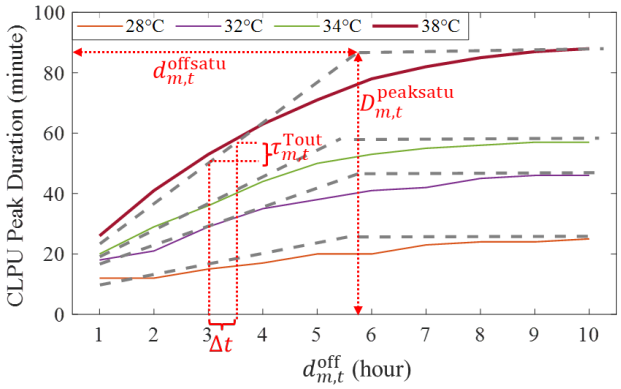


Fig. 5. Impact of outdoor temperature on CLPU duration curve ($\tau_{m,t}^{\text{Tout}} = \Delta d_{m,t}^{\text{peak}}/\Delta t$, where $\Delta t = 30$ minutes).

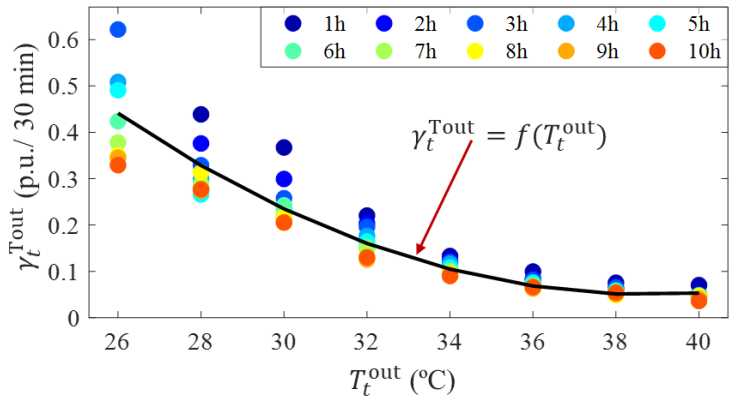


Fig. 6. Impact of outdoor temperature on CLPU decay rates. The dots represent decay rates obtained for different outage durations $d_{m,t}^{\text{off}}$ (Note that the curve is normalized to the synchronized CLPU peak, $P_{m,t}^{\text{MaxCLPU}}$).

*Step 4: Compute the CLPU decay rate*. As shown in Fig. 6, the CLPU power decay rate, $\gamma_{m,t}^{\text{Tout}}$, is a function of outdoor temperature, $T_t^{\text{out}}$. The higher $T_t^{\text{out}}$ is, the slower the CLPU peak decays from $P_m^{\text{MaxCLPU}}$ to the steady-state HVAC consumption level, $P_{m,t}^{\text{Steady}}$. Two curve-fitting approaches can be used for estimating the CLPU decay rate based on variations in downtime and ambient temperature. The first approach involves using one curve for each downtime to calculate the decay rate based on ambient temperature. The second approach is to use a single equivalent curve tailored to the most commonly occurring downtimes to determine the decay rate based on ambient temperature only.

Because the microgrid operators possess foreknowledge of the temperature variation range, we choose the second approach, using an equivalent 'decay rate-temperature' curve to estimate the decay rate based on $T_t^{\text{out}}$ to simplify the MGUC problem formulation and reduce computational complexity. To enhance the accuracy of decay rate estimation and minimize the impact of varying outage durations, we tailor the curve to best suit outage durations falling within the range of 4 to 10 hours. Please note that within our MGUC problem setting, short outages are seldom observed for two main reasons. First, minimum supply duration constraints are in place to discourage very brief CLPU events. Second, when considering the same total interruption duration, the CLPU consumption for multiple short interruptions is higher than that of a single long interruption (see Fig. 10(a)). As a result, the CLPU constraints favor scheduling a single, extended load shedding event rather than multiple shorter ones. Consequently, when short outages do occur, they typically happen only once during the daytime when temperatures exceed 30 ºC.

In practical applications, we recommend that modelers identify the temperature variation range and downtime range to select a 'decay rate-temperature' curve that best aligns with their specific operational conditions.

*Step 5: Formulate the adaptive CLPU model*. To facilitate the power calculation, we use $P_m^{\text{MaxCLPU}}$ as the power base so that the CLPU peak is 1.0 p.u., the power of the HVAC load of the $m^{\text{th}}$ LG at time $t$ is $k_{m,t}$ p.u., and the steady state power of the $m^{\text{th}}$ LG is $k_{m,t}^{\text{Steady}}$ p.u.. Let $t_{\text{O}}$, $t_{\text{H}}$, $t_{\text{D}}$, and $t_{\text{S}}$ be the interruption start time, the load restoration time (i.e., where the CLPU peak starts), the decay start time (i.e., where the CLPU peak ends), and the time reaching steady (see Fig. 7(c)).

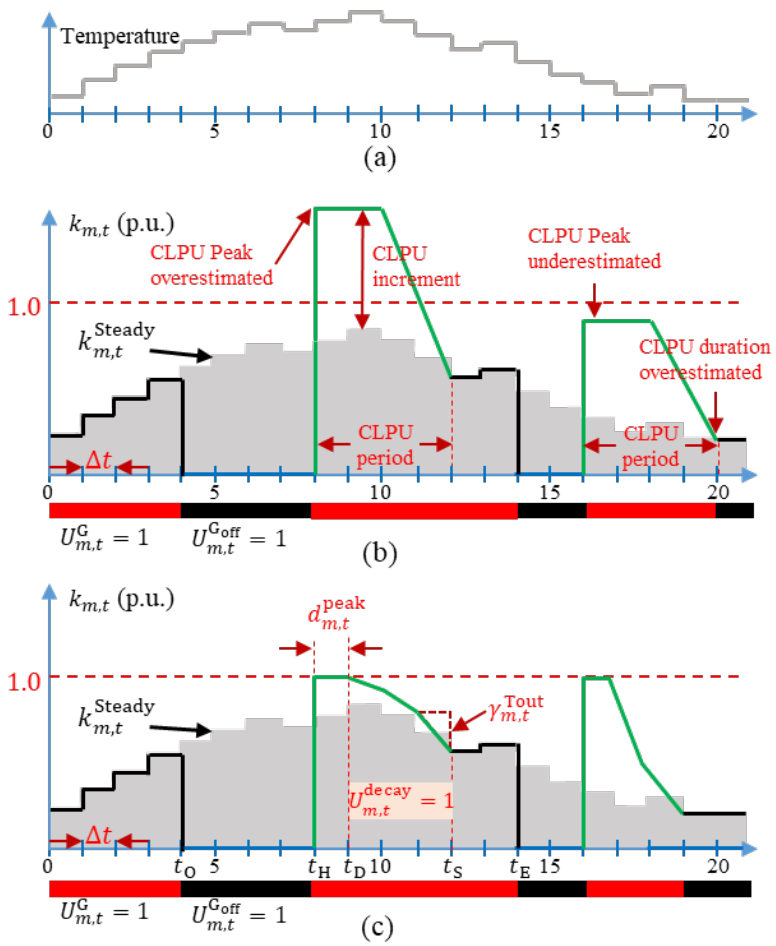


Fig. 7. Conceptual comparison of the CLPU models. (a) Temperature, (b) the fixed CLPU model (assuming the CLPU peak power is equal to twice that of the normal load and peak duration is 2 hours), (c) the adaptive CLPU model. Grey shaded areas are the HVACs' normal electricity consumption when there is no interruption.

The adaptive CLPU model can be described by

$$d_{m,t_{\text{H}}}^{\text{peak}} = \begin{cases} \sum_{t=t_{\text{O}}}^{t_{\text{H}}} \tau_{m,t}^{\text{Tout}}, d_{m,t_{\text{D}}}^{\text{peak}} < D_{m,t}^{\text{peaksatu}} \\ D_{m,t}^{\text{peaksatu}}, d_{m,t_{\text{D}}}^{\text{peak}} \geq D_{m,t}^{\text{peaksatu}} \end{cases} \tag{9-1}$$

$$t_{\text{D}} = t_{\text{H}} + d_{m,t_{\text{H}}}^{\text{peak}} \tag{9-2}$$

$$\sum_{t=t_{\text{D}}}^{t_{\text{S}}} \gamma_{m,t} = 1 - k_{m,t_{\text{S}}}^{\text{Steady}} \tag{9-3}$$

$$k_{m,t} = \begin{cases} 0, & t \in (t_{\text{O}}, t_{\text{H}}) \\ 1, & t \in [t_{\text{H}}, t_{\text{D}}] \\ 1 - \sum_{t=t_{\text{D}}}^{t} \gamma_{m,t}, t \in (t_{\text{D}}, t_{\text{S}}) & \\ k_{m,t}^{\text{Steady}}, & t \in [t_{\text{S}}, t_{\text{E}}] \end{cases} \tag{9-4}$$

$$k_{m,t}^{\text{CLPU}} = \begin{cases} 0, & t \in [t_{\text{O}}, t_{\text{H}}) \\ k_{m,t} - k_{m,t}^{\text{Steady}}, t \in [t_{\text{H}}, t_{\text{E}}] & \end{cases} \tag{9-5}$$

Figure 7 illustrates the daily ambient temperature profile (Fig. 7(a)), the fixed CLPU curve obtained by the

existing CLPU model (Fig. 7(b)), and the adaptive CLPU curve obtained by the proposed method (Fig. 7(c)). The fixed CLPU curve is obtained by modeling the HVAC operation for predefined outage duration and constant ambient temperature [7-8], so it has the fixed CLPU peak ratio (peak versus steady value), the fixed peak duration and decay duration for all outage scenarios. As shown in Fig. 7(b), the drawbacks of using such an approach are: 1) the CLPU peak can be significantly over- (hours 8-10) or under- (hours 16-17) estimated, and 2) significant over- or under- estimation of the CLPU decay energy needs.

The CLPU curves calculated by the adaptive model are illustrated in Fig. 7(c). Compared to the fixed CLPU, the adaptive CLPU model can accurately capture the CLPU energy needs by estimating the CLPU peak ratio based on $P_m^{\mathrm{MaxCLPU}}$ and $k_{m,t}^{\mathrm{Steady}}$ and calculating the accumulative impact of interruption duration and ambient temperature on peak duration by (9-1) and on the decay process by (9-4).

Note that when the ambient temperature varies a lot during the CLPU event, the CLPU peak duration and the decay duration vary too, the decay process may exhibit either a convex or concave shape, as shown in the first and second CLPU events in Fig.7(c), respectively.

The proposed adaptive CLPU model offers a more comprehensive and precise depiction of CLPU, encompassing ambient temperature, outage duration, and peak characteristics. All the necessary parameters for this adaptive model can be derived from offline HVAC simulations. As demonstrated in the following section, the model's linearization and cumulative formulation simplify the estimation of CLPU requirements when scheduling multiple load shedding events in the MGUC problem, all without imposing significant computational overhead.

### 2.4 Integration of the CLPU model into the 1st stage MGUC

The key challenge for considering the CLPU power and energy needs in MGUC is that the time when the load shedding happens and ends are decision variables so they are unknown before solving the MGUC problem. The main contribution of the proposed adaptive CLPU mode is that it provides an analytic formulation of the CLPU model with respect to the interruption duration and ambient temperature. This enables the MGUC to estimate the CLPU consumption during the optimization instead of using a predefined CLPU profile.

The adaptive CLPU model can be integrated into the MGUC as follows.

*Step 1: Determine the CLPU Peak Duration.*

$$U_{m,t}^{\mathrm{G_{off}}} = 1 - U_{m,t}^{\mathrm{G}} \tag{10}$$

$$0 \le d_{m,t} \le M U_{m,t}^{\mathrm{G_{off}}} \tag{11}$$

$$d_{m,t} + M U_{m,t}^{\mathrm{G}} \ge d_{m,t-1} + \tau_{m,t}^{\mathrm{Tout}} U_{m,t}^{\mathrm{G_{off}}} \Delta t \tag{12}$$

$$U_m^{\mathrm{satu}} \le U_{m,t}^{\mathrm{off}} \tag{13}$$

$$d_{m,t}^{\mathrm{peak}} \ge D_{m,t}^{\mathrm{peaksatu}} U_{m,t}^{\mathrm{satu}} \tag{14}$$

$$d_{m,t}^{\mathrm{peak}} \ge d_{m,t} - M U_{m,t}^{\mathrm{satu}} \tag{15}$$

$$d_{m,t}^{\mathrm{re}} - d_{m,t-1}^{\mathrm{re}} \ge d_{m,t-1}^{\mathrm{peak}} - U_{m,t-1}^{\mathrm{G}} \Delta t - M U_{m,t}^{\mathrm{G_{off}}} \tag{16}$$

$$0 \le d_{m,t}^{\mathrm{re}} \le M U_{m,t}^{\mathrm{G}} \tag{17}$$

Equation (10) determines whether an LG is "off". (11) and (13) ensure if the LG is "on", $d_{m,t}$ and the CLPU peak saturation status ($U_m^{\mathrm{satu}}$) should be 0. This is because the CLPU cumulates only when the LG is off. Thus, for each consecutive "off" interval, a resultant CLPU peak duration increment is added to the previous CLPU peak duration cumulatively using (12). Note that in (12), we do not consider the saturation effect.

Equations (14) and (15) are used for computing the CLPU peak duration considering whether or not the

peak duration is saturated. If the CLPU peak duration is saturated ($U_m^{\mathrm{satu}} = 1$), (15) will be disabled so (14) is used to calculate the saturated CLPU peak duration and saturation status. If the CLPU peak duration is NOT saturated ($U_m^{\mathrm{satu}} = 0$), (14) is disabled and (15) is used to compute the $d_{m,t}^{\mathrm{peak}}$ by $d_{m,t}$. Note that the maximum CLPU peak duration is capped according to the temperature of the step (see Fig. 5). The big-M method is used in (11-12) and (15-17), the $M$ is a selected large number greater than $24 \times 60$ minutes (in our case, $M$ =1500).

Equations (16) and (17) estimate the remaining CLPU peak durations when the LG is "on" and determine when the CLPU peak ends and the CLPU decay starts. Note that minimizing the duration of CLPU peaks can also minimize the additional energy required for CLPU. In (16), if the LG is turned "on" at step $t$, the remaining peak duration $d_{m,t}^{\mathrm{re}}$ should equal the estimated peak duration $d_{m,t-1}^{\mathrm{peak}}$; if the LG is turned "on" before step $t$ and remains "on" for the next time step, $d_{m,t}^{\mathrm{re}} = d_{m,t-1}^{\mathrm{re}} - \Delta t$. Thus, by incorporating those constraints, MGUC tends to supply loads in consecutive intervals rather than turning them on/off frequently.

*Step 2: Determine the CLPU Decay Process.* The following constraints compute CLPU decay status ($U_{m,t}^{\mathrm{decay}}$) for the $m^{\mathrm{th}}$ LG at time $t$ and ensure that the CLPU decay starts only when the CLPU peak duration elapses.

$$U_{m,t}^{\mathrm{decay}} \le U_{m,t}^{\mathrm{G}} \tag{18}$$

$$M\left(1 - U_{m,t}^{\mathrm{decay}}\right) \ge d_{m,t}^{\mathrm{re}} \tag{19}$$

$$-MU_{m,t}^{\mathrm{decay}} + M^{\mathrm{s}}U_{m,t}^{\mathrm{G}} \le d_{m,t}^{\mathrm{re}} \tag{20}$$

Equation (18) indicates that CLPU decay only could happen when the LG is "on". The decay status is decided by $d_{m,t}^{\mathrm{re}}$ and the LG status $U_{m,t}^{\mathrm{G}}$ with (19-20), if the CLPU peak is ended ($d_{m,t}^{\mathrm{re}} = 0$) and the LG is still served, $U_{m,t}^{\mathrm{decay}}$ is 1. Especially, $M^{\mathrm{s}}$ is a small constant (in our case, $M^{\mathrm{s}} = 0.001$).

*Step 3: Determine the CLPU Power Consumption.* From Fig. 4, $P_{m,t}^{\mathrm{Steady}}$ is estimated based on $T_t^{\mathrm{out}}$. Then, the steady load factor, $k_{m,t}^{\mathrm{Steady}}$, can be calculated by

$$k_{m,t}^{\mathrm{steady}} = \frac{P_{m,t}^{\mathrm{Steady}}}{P_m^{\mathrm{MaxCLPU}}} \tag{21}$$

where the TCL load factor $k_{m,t}$ is within the peak value (1.0 p.u.) when the LG is "on" and is bounded by

$$k_{m,t}^{\mathrm{steady}}U_{m,t}^{\mathrm{G}} \le k_{m,t} \le U_{m,t}^{\mathrm{G}} \tag{22}$$

When the LG is turned "on" at $t$, CLPU is at its peak so that $k_{m,t} = 1$ (1.0 p.u.), which could be ensured by $k_{m,t} = U_{m,t}^{\mathrm{G}} - U_{m,t-1}^{\mathrm{G}}$. During the CLPU peak duration, $k_{m,t} = 1$ is maintained. When the CLPU decay period starts, $k_{m,t} = k_{m,t-1} - \gamma_{m,t}U_{m,t}^{\mathrm{decay}}$. Note that reducing $k_{m,t}$ could mitigate CLPU, so all these scenarios can be ensured by

$$k_{m,t} - k_{m,t-1} \ge \left(U_{m,t}^{\mathrm{G}} - U_{m,t-1}^{\mathrm{G}}\right) - \gamma_{m,t}U_{m,t}^{\mathrm{decay}} \tag{23}$$

Thus, the CLPU increment factor, $k_{m,t}^{\mathrm{CLPU}}$, can be calculated by

$$k_{m,t}^{\mathrm{CLPU}} = k_{m,t} - k_{m,t}^{\mathrm{steady}}U_{m,t}^{\mathrm{G}} \tag{24}$$

Assuming that the CLPU peak is $P_{m,p}^{\mathrm{MaxCLPU}}$, the CLPU power increment in kW value, $P_{m,t}^{\mathrm{CLPU}}$, is calculated as

$$P_{m,p,t}^{\mathrm{CLPU}} = k_{m,t}^{\mathrm{CLPU}}P_{m,p}^{\mathrm{MaxCLPU}} \tag{25}$$

*Step 4: CLPU Penalty Terms.* To minimize CLPU impact on MGUC scheduling, we formulate a CLPU penalty term, $f_1^{\mathrm{CLPU}}$, consisting of three penalty factors, $c_{\mathrm{e}}^{\mathrm{CLPU}}$, $c_{\mathrm{dp}}^{\mathrm{CLPU}}$and $c_{\mathrm{re}}^{\mathrm{CLPU}}$ into the 1st stage MGUC formulation as:

$$f_1^{\mathrm{CLPU}} = \sum_{t=1}^{N_t} \sum_{m=1}^{N^G} \left( c_{\mathrm{e}}^{\mathrm{CLPU}} P_{m,t}^{\mathrm{CLPU}} \Delta t + c_{\mathrm{dp}}^{\mathrm{CLPU}} d_{m,t}^{\mathrm{peak}} + c_{\mathrm{re}}^{\mathrm{CLPU}} d_{m,t}^{\mathrm{re}} \right) \tag{26}$$

$$P_{m,p,t}^{\mathrm{norm}} = P_{m,p,t}^{\mathrm{Ncrit}} + P_{m,p,t}^{\mathrm{crit}} \tag{27}$$

$$\sum_{l \in \Omega_m^{\mathrm{from}}} P_{lm,p,t} = U_{m,t}^{\mathrm{G}} P_{m,p,t}^{\mathrm{norm}} + \boldsymbol{P_{m,p,t}^{\mathrm{CLPU}}} + \sum_{n \in \Omega_m^{\mathrm{to}}} P_{mn,p,t} \tag{28}$$

Equation (28) ensures that each phase meets the power balance requirement when considering the CLPU effect. Note that the CLPU power needs can exacerbate 3-phase load unbalance. Because the adaptive CLPU can accurately estimate the per-phase CLPU power, it can be used for improving the phase unbalance control. This is another advantage of using the adaptive CLPU model in MGUC in unbalanced distribution systems.

### 2.5 The 2nd Stage MGUC Problem Formulation

The objective function of the 2nd stage MGUC minimizes the amount of per-phase DR usage, $f_2^{\mathrm{DR}}$, the PV curtailment, $f_2^{\mathrm{PV}}$, and the BESS negative energy deviation from its budget, $f_2^{\mathrm{BESS}}$.

$$\min \ f_2^{\mathrm{DR}} + c_2^{\mathrm{low}} f_2^{\mathrm{BESS}} + c_2^{\mathrm{PV}} f_2^{\mathrm{PV}} \tag{29}$$

$$f_2^{\mathrm{DR}} = \sum_{t'=1}^{T_2} \sum_{m=1}^{N^{\mathrm{G}}} \sum_{i=1}^{N_m^{\mathrm{node}}} \sum_{p \in \{a,b,c\}} U_{m,i,p,t'}^{\mathrm{DR}} P_{m,i,p,t'}^{\mathrm{node}} \Delta t' \tag{30}$$

$$P_{m,i,p,t'}^{\mathrm{node}} = P_{m,i,p,t'}^{\mathrm{norm}} + k_{m,t'}^{\mathrm{CLPU}} P_{m,i,p}^{\mathrm{MaxCLPU}} \tag{31}$$

$$f_2^{\mathrm{BESS}} = \Delta E_2^{\mathrm{low}} \tag{32}$$

$$E_{2,T_2} + \Delta E_2^{low} \geq E_1 \tag{33}$$

$$\Delta E_2^{\mathrm{low}} \geq 0 \tag{34}$$

$$f_2^{\mathrm{PV}} = 3 \sum_{t'=1}^{T_2} P_{\mathrm{pv},\,t'}^{\mathrm{curt}} \Delta t' \tag{35}$$

The CLPU effect is included by (31) in the 2nd stage, the CLPU factor, $k_{m,t'}^{\mathrm{CLPU}}$, is calculated by interpolating the first stage's estimated CLPU factor $k_{m,t}^{\mathrm{CLPU}}$ linearly. We penalize the negative BESS energy deviations with (32-34) as such deviations could compromise the overall optimal solution of the 1st stage.

In the 2nd stage, we perform the unbalanced linear power flow [29]. The hybrid PV plant's voltage is fixed at 1.03 p.u., and all other nodal voltages are maintained within the range of [0.95,1.05] p.u.. The operational constraints of PV and BESS, microgrid reserve constraints, and linearization of active power and reactive power constraints of inverters and lines are similar to those in the 1st stage.

## 3. Simulation Results

As shown in Fig. 1, the feeder-level microgrid is modeled by the modified IEEE 123-bus test system. The microgrid is supplied by a hybrid PV plant (Node 7) consisting of a 4.5 MW PV farm and a 3 MW/6 MWh BESS. A prolonged outage occurs and the hybrid PV cannot provide service in the first several hours due to the

extreme weather condition and system device repair, then the hybrid PV plant is expected to serve the feeder in the next 48 hours. As the only grid-forming source, the BESS regulates the system voltage at 1.03 p.u. and has a charging/discharging efficiency of 95% with a state of charge (SOC) operational range of 20% to 90%. The initial SOC is set at 90%. We use the actual PV forecasts and measurements obtained from a 5MW PV farm in this study. The forecasting error is small on the first day but significantly larger on the second day, as depicted in Fig. 8.

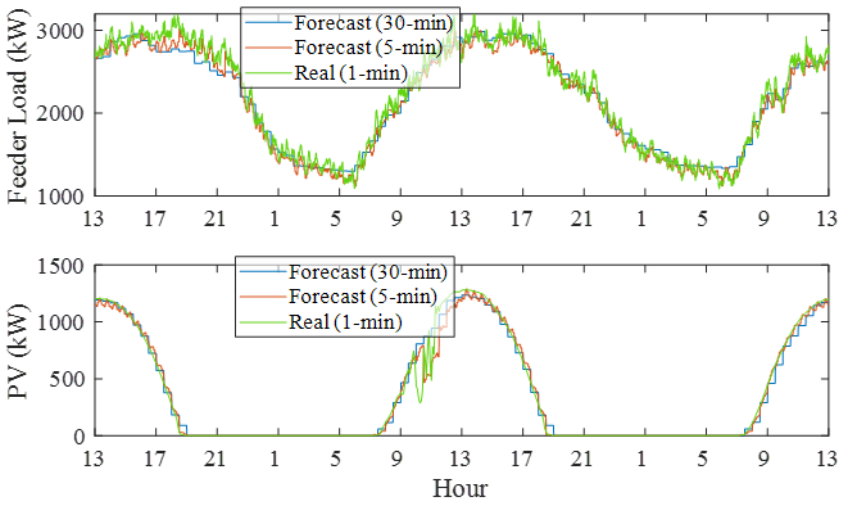


Fig. 8. Total feeder normal load and per-phase PV profiles (forecasted and real) on the 123-bus feeder.

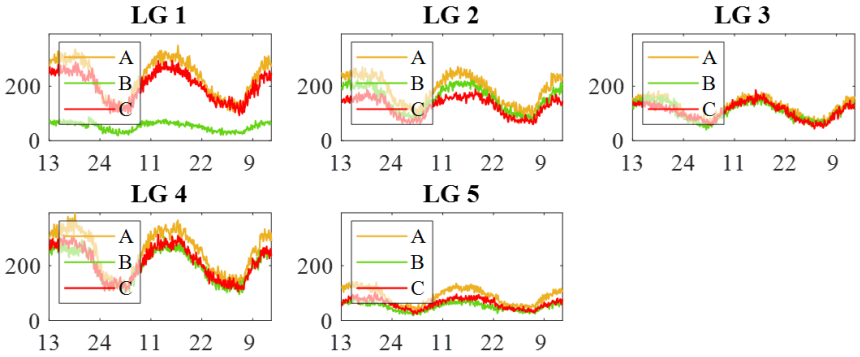


Fig. 9. Per-phase 5-min normal load for the five load groups.

There are two customer-preferred service periods: 7:00-9:00 and 18:00-20:00, each assigned a preferred time weighting ($w_t^{\text{pref}}$) of 1.5. Critical loads (Nodes 47 and 65) are assigned with a priority weighting ($w_{m,p}^{\text{crit}}$) of 4. The load at each load node is obtained by randomly selecting the load profiles from the Pecan Street dataset [25], which provides minute-level submeter data, using methods described in [22]. The total loads comprise two parts: the non-HVAC load and the HVAC load. The baseload (i.e. non-HVAC load) is forecasted using the method introduced in [30]. The 1100 heterogeneous HVAC units are modeled by the RCQ model, the parameters of which are derived from the sub-metered HVAC load profiles (also from the Pecan Street dataset) using methods introduced in [26].

The HVAC load consumptions under different outage durations and ambient temperatures are used to derive the parameters of the adaptive CLPU model using the methods introduced in Section 2.3. Note that the CLPU model parameters are in per unit value, so all LGs share a similar set of parameters, except for $P_{m,p}^{\text{MaxCLPU}}$ and $P_{m,t}^{\text{Steady}}$, which is related to the number of HVAC units inside each LG. It is worth noticing that the 3-phase loads within some LGs can exhibit substantial imbalances (e.g. LG1), as shown in Fig. 9.

The corresponding weather data are downloaded from NOAA. The parameters for MGUC, HVAC, and CLPU can be found in [31].

The MGUC algorithm is formulated as a MILP problem. The solver is CPLEX 12.10 on Matlab 2019. The computational environment is a desktop computer equipped with an Intel Core i9-9900 CPU and 64GB of RAM. The optimality gap is 0.01%. The MGUC-OpenDSS simulation is conducted using the Matlab COM interface.

We run the MGUC-OpenDSS co-simulation with MGUC using baseload forecast and estimating CLPU, and OpenDSS using actual baseload and simulated HVAC loads, both of which are 1-minute data. In the figures, "RT" denotes real-time simulation results from OpenDSS and "MGUC" denotes the 2nd stage MGUC dispatching results, and the red dashed rectangle denotes the preferred periods.

### 3.1 Verification of the Adaptive CLPU Model Performance

To verify the performance of the adaptive CLPU model, in Fig. 10, the simulation results of three constant ambient temperature cases are shown. In each case, we model three CLPU events, the duration of which is 2-hour, 4-hour, and 8-hour duration, respectively. The actual HVAC consumption is simulated by 1100 heterogeneous HVAC models.

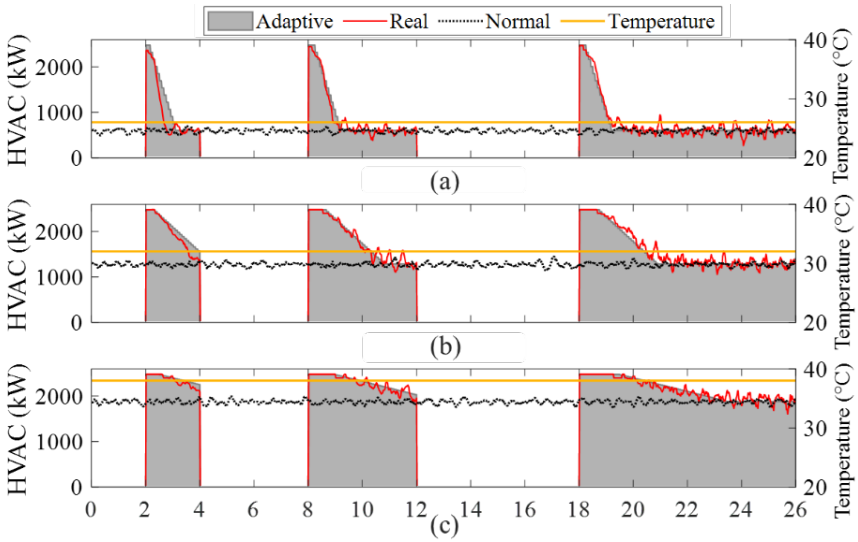


Fig. 10. CLPU estimation using the adaptive CLPU model assuming the ambient temperature remains constant for the entire 26-hour period. (a) 26 °C, (b) 32 °C, (c) 38 °C. Note that the black line is the steady-state HVAC load. The three CLPU events represent three different outage durations: 2-hour, 4-hour, and 8-hour.

From the results, the following observations can be made:

- When the ambient temperature remains constant, the proposed adaptive CLPU model (the shaded areas) matches the actual HVAC load (the red lines) very well.
- As we stated in Section 2.3, if the ambient temperature is mild (i.e., 26ºC), the estimated CLPU peak is slightly higher than the actual peak when the interruption duration is only 2 hours. This is because we assume the CLPU peak equals to $P_m^{\mathrm{MaxCLPU}}$ for all scenarios in order to simplify the CLPU model representation.
- In Fig. 10 (a) and (b), we can observe a minor deviation in the first CLPU decay curve. This error occurs because the fitted curve for computing the decay rate (see Fig. 6) exhibits greater errors when the ambient temperature is 26ºC, making the calculated decay rate for a 2-hour outage duration lower than the actual value.

### 3.2 Comparison between Adaptive and Fixed CLPU Models

Next, we compare the performance between the adaptive and the fixed CLPU models assuming that the time and duration of the interruption as well as the ambient temperature profiles are known beforehand. In Fig. 11, it is evident that when the fixed CLPU model neglects temperature variations (as seen in the 'Fixed (temp)' case) or assumes a constant interruption duration (observed in the 'Fixed (otg)' case), the resulting CLPU curve (represented by the blue and green dashed lines in Fig. 11) demonstrates notable deviations from the actual curves (depicted by the red curve). Because both the timing and duration of interruptions are decision-dependent in MGUC, existing works [11-13] considering using fixed CLPU models could not achieve desirable results when scheduling multiple CLPU events in a prolonged scheduling horizon (e.g., 24 to 48 hours).

This also demonstrates a major drawback of using a fixed CLPU model: the establishment of a predetermined CLPU profile depends mainly on educated guesses, because before the MGUC is executed, when and for how long an LG will be powered off are unknown variables.

On the other hand, the adaptive CLPU model produces CLPU curves that closely match the actual ones. The time-varying temperature will impact the shape of the CLPU profile in terms of the peak duration, decay rate, and steady-state value. Note that if the temperature is increasing rapidly, the CLPU decay curve is convex due to the increase of the decay rate, for example, the second CLPU curve in Fig.11(a). However, if the temperature is decreasing rapidly, the CLPU decay curve will be concave due to the decreasing decay rate, as shown by the first CLPU in Fig.11(b).

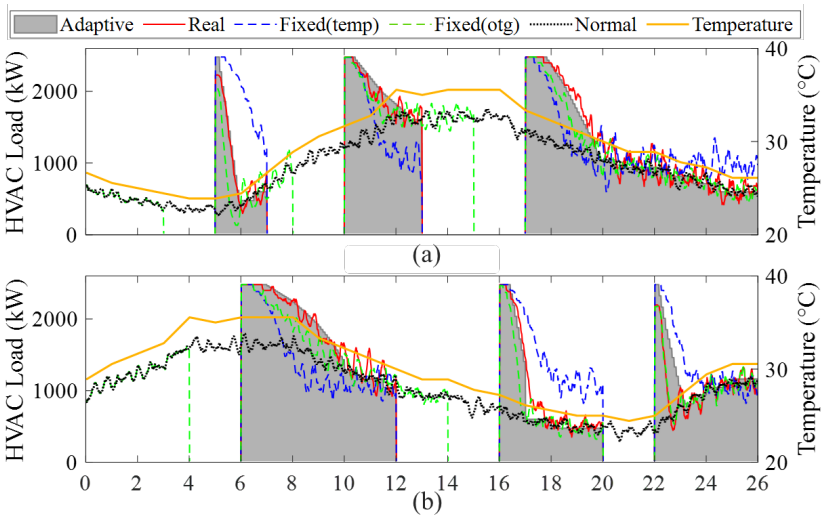


Fig. 11. Comparing various CLPU models for (a) a case with high daily temperatures occurring between hours 12 and 16, and (b) a case with high daily temperatures occurring between hours 4 and 8. Note that 'Fixed (temp)' denotes simulation results obtained by a fixed CLPU model derived from the average temperature over a 26-hour period; 'Fixed(otg)' denotes simulation results obtained by a fixed CLPU model assuming a 2-hour interruption duration.

### 3.3 CLPU Enhanced MGUC

As shown in Table II, three MGUC cases are set up for comparing the effect of modeling CLPU effects. We compare the MGUC results by evaluating MSD violation, energy served during customer-preferred periods, and total served critical load, and total served baseload. The simulation results are summarized in Tables III and

IV and shown in Figs. 12-17.

Table II. Microgrid unit commitment cases: with and without CLPU

| Case | CLPU Model |
|---|---|
| **1** | **NoCLPU**: do not consider the CLPU effect. |
| **2** | **FixCLPU**: fixed two-block model [12] with the CLPU increment equal to the baseload plus the normal HVAC load and a CLPU duration of 2 hours, these parameters are selected based on the average temperature 29 $^{o}$C. |
| **3** | **AdaptCLPU**: the proposed method considering the variation of the ambient temperatures and outage durations |

### *3.3.1 With and without CLPU*

From the simulation results, we made the following observations regarding the main drawbacks of ignoring CLPU (NoCLPU case):

- Less served critical loads and more CLPU consumption, as shown in Table III.
- Frequent LG switching actions. As shown in Fig. 12(a), there are multiple 30-minute or 1-hour supply periods, representing frequent interruptions of power supply for LGs 1-3 and more violations of MSD constraints (10 occurrences). This also leads to more CLPU events (14 occurrences) and consumption, as shown in Table III and Fig. 15(a).
- More violations of the operational constraints. As shown in Fig. 16 (a), failing to account for CLPU will cause the BESS SOC to drop significantly lower than the SOC lower limit.
- More forced interruptions. The microgrid has to be shut down twice during hours 9-12 on the second day after the SOC drops below 10%. This is because when picking up the "off" LGs, the scheduled energy budget for the 30-minute scheduling interval is quickly depleted by the additional CLPU power and energy needs, which is almost two times higher than the dispatched value (see Fig. 12(b)).
- In contrast, when the CLPU is considered in MGUC (FixCLPU and AdaptCLPU), the MSD constraints are satisfied with less frequent service interruptions (Fig. 13 and Fig. 14) and smaller BESS negative deviation (Fig. 16).

Table III. Microgrid performance comparison with and without CLPU

| Case | Served load (kWh) | Served load in preferred periods (kWh) | | Served critical load (kWh) | Served baseload (kWh) | Curtailed PV (kWh) | CLPU (kWh) | Estimated CLPU (kWh) |
|---|---|---|---|---|---|---|---|---|
| | | total | CLPU part | | | | | |
| NoCLPU | 54493 | **10196** | 1757 | 4734 | 21438 | 2999 | 7697 | - |
| FixCLPU [12] | 50737 | 7445 | 540 | 4814 | 20464 | 5877 | **5893** | 12885 |
| AdaptCLPU | **55173** | 7771 | 667 | **4857** | **22210** | **2591** | 6835 | 5565 |

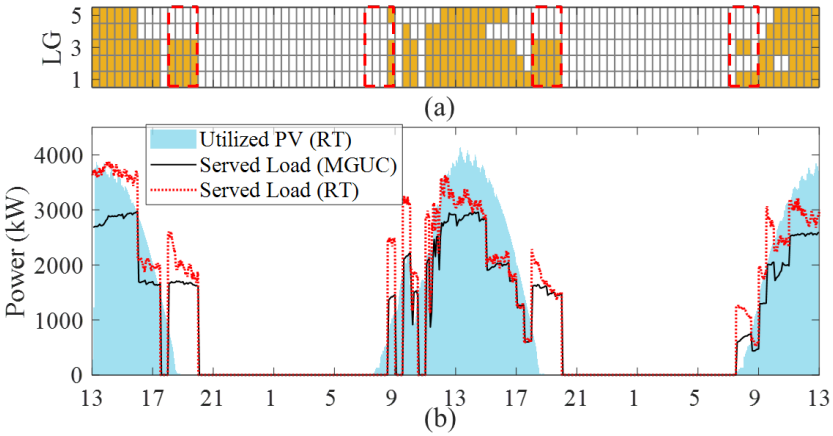


Fig. 12. Simulation results for **NoCLPU**. (a) LG status for each scheduling interval with shaded blocks as "on" blocks, (b) Profiles of the utilized PV, the MGUC-scheduled loads, and the actually served load.

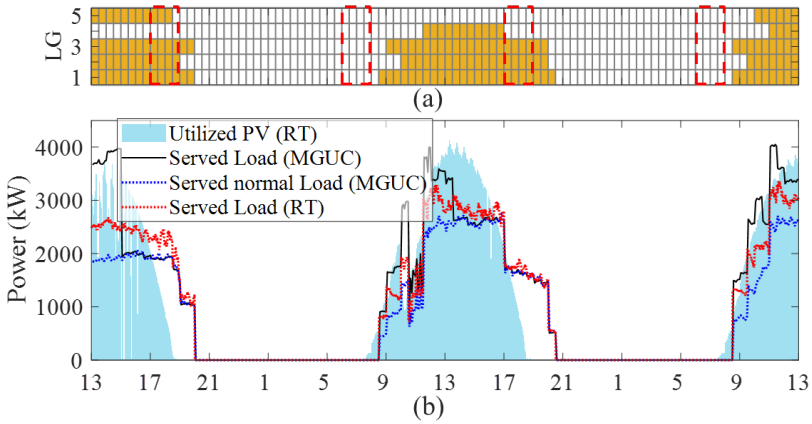


Fig. 13. Simulation results for **FixCLPU**. (a) LG status for each scheduling interval with shaded blocks as "on" blocks, (b) Profiles of the utilized PV, the MGUC-scheduled loads, and the actually served load.

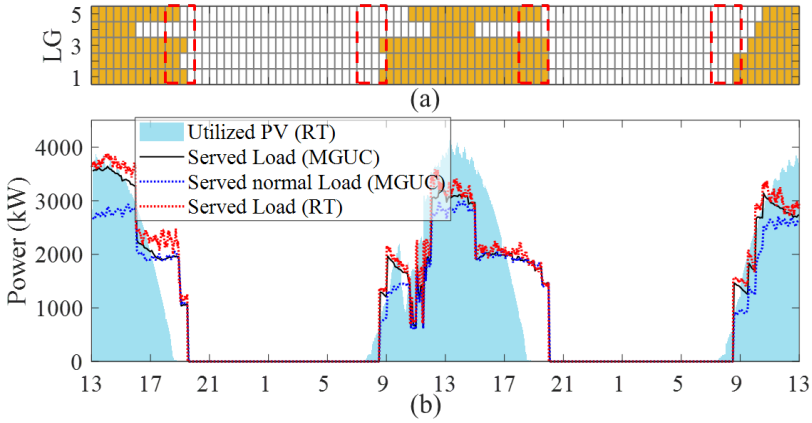


Fig. 14. Simulation results for **AdaptCLPU**. (a) LG status for each scheduling interval with shaded blocks as "on" blocks, (b) Profiles of the utilized PV, the MGUC-scheduled loads, and the actually served load.

### *3.3.2 CLPU Model Comparison: Fixed versus Adaptive*

From the simulation results, we made the following observations regarding the main drawbacks of fixed CLPU:

- FixCLPU tends to over-estimate (see Figs. 13(b) and 15(b)) or under-estimate the CLPU effect (see hours 15-17 on the first day in Fig. 13(b)).
- As shown in Table III, compared to AdaptCLPU, the imprecise CLPU predictions lead to reduced served load (-8%) and more PV curtailment (over 3.3 MWh), marking the poorest performance among the three algorithms.
- As shown in Fig. 16, FixCLPU has the highest SOC level since the actual SOC exceeds the scheduled value, primarily due to the overestimation of CLPU effect. This also results in PV curtailment during hours 13-17 on the first day.
- As depicted in Fig. 17, FixCLPU exhibits the biggest gap in LGs' served time, with LG 1 served for 23.5 hours and LGs 4 and 5 served for less than 8.5 hours. It exhibits a tendency to serve fewer LGs due to CLPU overestimation, for example, only 4 LGs can be served on the first day (refer to Fig. 13 (a)). While AdaptCLPU can provide service to all LGs each day and extend the service time for LG 5 to 17.5 hours (refer to Fig. 14 (a)).
- In contrast, adaptive-CLPU effectively captures both the magnitude and duration of CLPU events, resulting in a close alignment between actual served loads and the MGUC scheduled loads (refer to Fig. 14 (b) and Fig. 15 (c)) and the least BESS storage deviation (see Fig. 16). This alignment enables the optimization of the LG supply sequence across the entire scheduling horizon. As shown in Table III, the performance of the AdaptCLPU case outperforms the other two cases in all performance metrics except the "served loads in preferred periods" and "CLPU consumption".

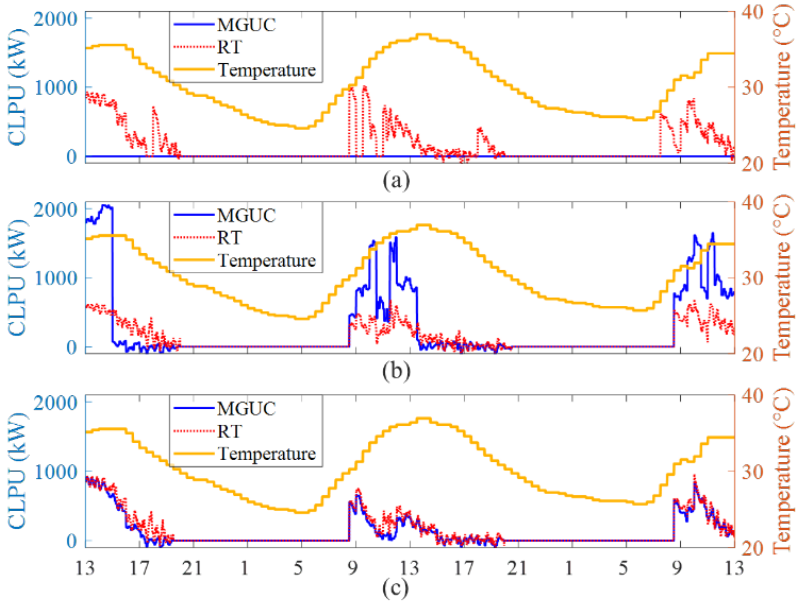


Fig. 15. MGUC estimated CLPU load versus the actual CLPU load (a) NoCLPU, (b) FixCLPU, and (c)AdaptCLPU.

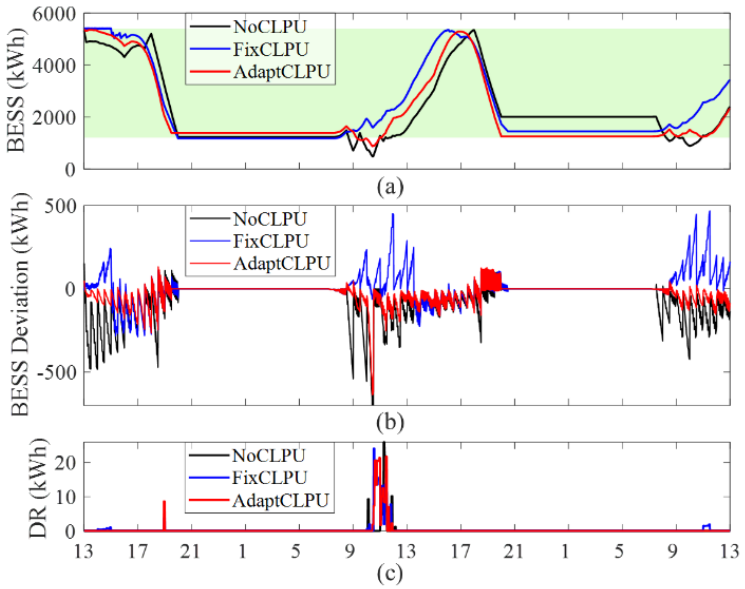


Fig. 16. Comparison of BESS and DR operation in the three cases (a) BESS energy storage with the shaded area denoting the operational range (b) Energy storage deviations (calculated by the MGUC scheduled BESS energy level minus the actual energy storage level), and (c) Actual DR usage.

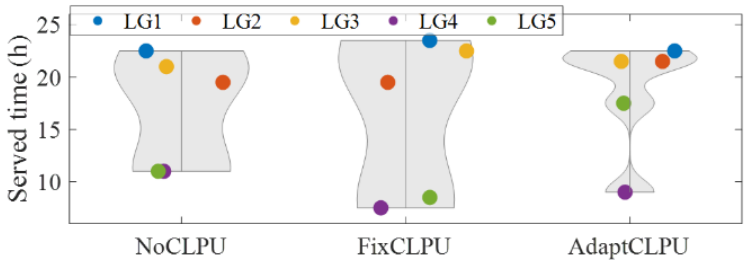


Fig. 17. Comparison of the LGs' served time of the three cases.

### *3.3.3 Computing Cost*

We compare the solving time for the 1st stage MGUC (the most intensive stage) when considering the CLPU effects. As Table IV indicates, the average runtime for AdaptCLPU is under 3.8 seconds, with a maximum runtime of 19.6 seconds. Therefore, despite the higher model complexity associated with the adaptive CLPU model compared to the FixCLPU and NoCLPU cases, the increase in runtime is not substantial and comfortably satisfies the runtime constraints for the 2-stage microgrid operation with 5-minute power dispatching requirements.

Table IV. Model Complexity and Runtime

| Case | Number of continuous variables | Number of binary variables | Number of constraints | Average calculation time | Max. calculation time |
|---|---|---|---|---|---|
| NoCLPU | 1472 | 800 | 4786 | 0.6 s | 1.8 s |
| FixCLPU | 1792 | 960 | 5408 | 1.0 s | 3.1 s |
| AdaptCLPU | 2112 | 1120 | 7328 | 3.8 s | 19.6 s |

## 4. Conclusions

In this study, we introduced an innovative adaptive CLPU model that incorporates ambient temperature and interruption duration as input variables, enabling precise estimation of CLPU power and energy requirements. Utilizing this adaptive CLPU model, we established a comprehensive set of operational constraints for the MILP MGUC framework. This novel approach empowers the MGUC system to autonomously calculate CLPU needs and optimize the LG on/off sequence effectively. Our simulation results shown that the adaptive CLPU enhanced MGUC surpasses the existing approaches, which either neglected CLPU or relied on fixed CLPU curves. By accurately addressing the demands of multiple CLPU events within the 1st stage energy scheduling process during extended outages, we significantly reduce power and energy shortfalls in real-time operations. This, in turn, leads to enhanced served total load, critical loads and baseloads, improved customer comfort (as the minimum service duration constraints are met), and fewer forced microgrid outages. Note that in our problem setting, an equivalent 'decay rate-temperature' curve is used for estimating decay rate estimation based on ambient temperature. To minimize the impact of varying downtime on the estimation accuracy, we customize the curve to optimally align with outage durations ranging from 4 to 10 hours. This approach proves effective in the proposed problem setting, primarily because short outages are infrequent due to the minimum service duration and CLPU constraints. In practice, to adapt the CLPU model effectively to various day types and MGUC problem settings, we advise modelers to customize the equivalent 'decay rate-temperature' curve to best capture the temperature range and outage duration characteristics specific to their scenarios.

Our future research will focus on the development of MGUC algorithms for managing multiple feeders with multiple grid-forming sources. This broader scope promises to further advance the reliability, resiliency, and robustness of microgrid energy management systems in prolonged outages.

## 5. Acknowledgement

This research is supported by the U.S. Department of Energy's Office of Energy Efficiency and Renewable Energy (EERE) under the Solar Energy Technologies Office Award Number DE-EE0008770.

## 6. References

[1] Berry R, U.S. electricity customers averaged seven hours of power interruptions in 2021, Nov. 14, 2022. [Online]. Available: https://www.eia.gov/todayinenergy

[2] Hussain A, Bui V-H, Kim H-M. Microgrids as a resilience resource and strategies used by microgrids for enhancing resilience. Applied Energy 2019;240:56–72. doi:10.1016/j.apenergy.2019.02.055.

[3] Solar Energy Industries Association, Solar market insight report 2022 Q2, Jun. 7, 2022. [Online]. Available: https://www.seia.org/research-resources/solar-market-insight-report-2022-q2.

[4] U.S. Energy Information Administration, Heating and cooling no longer majority of U.S. home energy use, Mar. 7, 2013, [Online]. Available: https://www.eia.gov/todayinenergy/detail.php?id=10271.

[5] Gilvanejad M, Askarian Abyaneh H, Mazlumi K. Estimation of cold-load pickup occurrence rate in distribution systems. IEEE Transactions on Power Delivery 2013;28:1138–47. doi:10.1109/tpwrd.2012.2231967.

[6] Bu F, Dehghanpour K, Wang Z, Yuan Y. A data-driven framework for assessing cold load pick-up demand in service restoration. IEEE Transactions on Power Systems 2019;34:4739–50. doi:10.1109/tpwrs.2019.2922333.

[7] Lang W, Anderson M, Fannin D. An analytical method for quantifying the electrical space heating component of a cold load pick up. IEEE Transactions on Power Apparatus and Systems 1982;PAS-101:924–32. doi:10.1109/tpas.1982.317158.

[8] Aubin J, Bergeron R, Morin R. Distribution transformer overloading capability under cold-load pickup conditions. IEEE Transactions on Power Delivery 1990;5:1883–91. doi:10.1109/61.103685.

[9] Schneider KP, Sortomme E, Venkata SS, Miller MT, Ponder L. Evaluating the magnitude and duration of cold load pick-up on residential distribution feeders using multi-state load models. IEEE Transactions on Power Systems 2016;31:3765–74. doi:10.1109/tpwrs.2015.2494882.

[10] McDonald J, Bruning A. Cold load pickup. IEEE Transactions on Power Apparatus and Systems 1979;PAS-98:1384–6. doi:10.1109/tpas.1979.319340.

[11] Chen B, Chen C, Wang J, Butler-Purry KL. Multi-time step service restoration for advanced distribution systems and Microgrids. IEEE Transactions on Smart Grid 2018;9:6793–805. doi:10.1109/tsg.2017.2723798.

[12] Arif A, Ma S, Wang Z, Wang J, Ryan SM, Chen C. Optimizing service restoration in distribution systems with uncertain repair time and demand. IEEE Transactions on Power Systems 2018;33:6828–38. doi:10.1109/tpwrs.2018.2855102.

[13] Arif A, Wang Z, Chen C, Wang J. Repair and resource scheduling in unbalanced distribution systems using neighborhood search. IEEE Transactions on Smart Grid 2020;11:673–85. doi:10.1109/tsg.2019.2927739.

[14] Song M, nejad RR, Sun W. Robust distribution system load restoration with time-dependent cold load pickup. IEEE Transactions on Power Systems 2021;36:3204–15. doi:10.1109/tpwrs.2020.3048036.

[15] Li YL, Sun W, Yin W, Lei S, Hou Y. Restoration strategy for active distribution systems considering endogenous uncertainty in cold load pickup. IEEE Transactions on Smart Grid 2022;13:2690–702. doi:10.1109/tsg.2021.3120555.

[16] Arif A, Wang Z. Networked microgrids for service restoration in resilient distribution systems. IET Generation, Transmission & Distribution 2017;11:3612–9. doi:10.1049/iet-gtd.2017.0380.

[17] Mousavizadeh S, Haghifam M-R, Shariatkhah M-H. A linear two-stage method for resiliency analysis in distribution systems considering renewable energy and Demand Response Resources. Applied Energy 2018;211:443–60. doi:10.1016/j.apenergy.2017.11.067.

[18] Chen B, Chen C, Wang J, Butler-Purry KL. Sequential Service Restoration for unbalanced distribution systems and microgrids. IEEE Transactions on Power Systems 2018;33:1507–20. doi:10.1109/tpwrs.2017.2720122.

[19] Xu Y, Liu C-C, Schneider KP, Tuffner FK, Ton DT. Microgrids for service restoration to critical load in a resilient distribution system. IEEE Transactions on Smart Grid 2018;9:426–37. doi:10.1109/tsg.2016.2591531.

[20] Fobes DM, Nagarajan H, Bent R. Optimal microgrid networking for maximal load delivery in phase unbalanced distribution grids: A declarative modeling approach. IEEE Transactions on Smart Grid 2023;14:1682–91. doi:10.1109/tsg.2022.3208508.

[21] Wang Z, Wang J, Chen C. A three-phase microgrid restoration model considering unbalanced operation of distributed generation. IEEE Transactions on Smart Grid 2018;9:3594–604. doi:10.1109/tsg.2016.2621412.

[22] Hu R, Li Y, Zhang S, Shirsat A, Muthukaruppan V, Tang W, et al. A load switching group based feeder-level Microgrid Energy Management Algorithm for service restoration in Power Distribution System. 2021 IEEE Power & Energy Society General Meeting (PESGM) 2021. doi:10.1109/pesgm46819.2021.9638231.

[23] 123-Bus Feeder, Jan. 2021, [online], Available: https://cmte.ieee.org/pes-testfeeders/resources/.

[24] Du P, Lu N, Zhong H, Demand response in smart grids.Cham: Springer, 2019.

[25] Pecan Street dataset, Oct. 2020, [online]: http://www.pecanstreet.org/

[26] Lu J. Modeling and controller design of a community microgrid. dissertation. North Carolina State University, NC, USA, 2018.

[27] Liang M, Meng Y, Lu N, Lubkeman D, Kling A. HVAC load disaggregation using low-resolution smart meter data. 2019 IEEE Power & Energy Society Innovative Smart Grid Technologies Conference (ISGT) 2019. doi:10.1109/isgt.2019.8791578.

[28] Kim H, Ye K, Lee HP, Hu R, Lu N, Wu D, et al. An ICA-based HVAC load disaggregation method using Smart Meter Data. 2023 IEEE Power & Energy Society Innovative Smart Grid Technologies Conference (ISGT) 2023. doi:10.1109/isgt51731.2023.10066402.

[29] Bassey O, Chen C, Butler-Purry KL. Linear power flow formulations and optimal operation of three-phase autonomous droop-controlled microgrids. Electric Power Systems Research 2021;196:107231. doi:10.1016/j.epsr.2021.107231.

[30] Li Y, Zhang S, Hu R, Lu N. A meta-learning based distribution system load forecasting model selection framework. Applied Energy 2021;294:116991. doi:10.1016/j.apenergy.2021.116991.

[31] https://github.com/rxhu89/paper_parameter_MGUC_CLPU